

# Information Content of the Cosmic Web

Juan García-Bellido<sup>1</sup>

<sup>1</sup>*Instituto de Física Teórica UAM/CSIC, Universidad Autónoma de Madrid, Cantoblanco 28049 Madrid, Spain*

(Dated: May 26, 2026)

We present an information-theoretic analysis of the Cosmic Web that goes beyond the scalar density contrast and exploits the full structure of the tidal deformation tensor. The three eigenvalues  $(\lambda_1, \lambda_2, \lambda_3)$  of the tidal Hessian furnish a natural morphological classifier: clusters, filaments, walls, and voids correspond to  $(+, +, +)$ ,  $(+, +, -)$ ,  $(+, -, -)$ , and  $(-, -, -)$  sign patterns, and their joint probability distribution function (PDF), known analytically in the linear regime from Doroshkevich (1970), defines a continuous Shannon entropy that quantifies the information encoded in the geometry of large-scale structure. Additional information resides in the shear invariants  $\mathcal{Q} = \text{Tr}(\mathbf{T}^2)$  and  $\mathcal{A} = \text{Tr}(\mathbf{T}^3)$ , which are algebraically independent of the density contrast  $\delta$  and capture anisotropic deformation invisible to the density alone. The information dimension of each morphological component is related to its Hausdorff (fractal) dimension through the multifractal formalism: clusters ( $D_H \approx 1.2$ ), filaments ( $D_H \approx 1.8$ ), walls ( $D_H \approx 2.5$ ), and voids ( $D_H \approx 3$ ) define a spectrum of generalized Rényi dimensions  $D_q$ , whose  $q \rightarrow 1$  limit recovers the Shannon information dimension. The resulting entropy budget identifies filaments as the dominant information carriers of the matter distribution, while the tidal eigenvalue entropy is maximized in wall-like configurations near the saddle points of the gravitational potential. We also compute the redshift evolution of the multifractal entropy and derive its relation to the linear growth rate  $f(z)$ , providing an independent constraint complementary to redshift-space-distortion measurements of  $f\sigma_8$ .

PACS numbers: 98.65.-r, 89.70.Cf, 98.80.-k, 05.45.Df

## I. INTRODUCTION

The large-scale structure of the Universe—the Cosmic Web—organises itself into a hierarchy of morphological components: vast, nearly empty voids; thin planar walls; elongated filaments; and dense, compact galaxy clusters at their intersections [1, 2]. This four-component classification, pioneered by the Zel’dovich approximation [3] and formalized by the tidal-field eigenvalue signature [4] and the NEXUS scheme [5], provides a natural partition of the cosmic density field.

The density contrast  $\delta \equiv \rho/\bar{\rho} - 1$  is the most commonly used scalar characterization of large-scale structure. However,  $\delta$  captures only the trace of the tidal deformation tensor,  $I_1 \equiv \text{Tr}(\Psi)$ ; the two remaining independent invariants—the squared shear  $I_2 \equiv [(\text{Tr} \Psi)^2 - \text{Tr}(\Psi^2)]/2$  and the cubic invariant  $I_3 \equiv \text{Tr}(\Psi^3)$ —encode anisotropic information about the geometry of collapse that is invisible to the density alone.

Several authors have previously brought information-theoretic tools to bear on large-scale structure. Hosoya, Buchert & Morita [6] introduced the Kullback–Leibler relative information entropy as a measure of distinguishability of the inhomogeneous density field from its spatial average, and studied its time evolution in the linear regime; subsequent work extended this to nonlinear clustering and the role of a cosmological constant [7]. Pandey [8] used Shannon entropy of the density field to test cosmic homogeneity in the SDSS galaxy catalog, spawning a series of studies of isotropy, bias and non-Gaussianity. Leclercq et al. [9] introduced a decision-theoretic framework that uses mutual information and

the Jensen–Shannon divergence to compare T-web, DIVA and ORIGAMI classifiers [10] on SDSS reconstructions, asking which segmentation retains the most cosmological information for parameter inference, model selection and prediction. Graph entropy of the cosmic-web network has been shown to discriminate cosmological parameters and redshift evolution at the  $10^{-2}$ -bit level [11]. Vazza [12, 13] applied statistical complexity and block entropy to cosmological simulations, estimating that the thermal and kinetic energy fields require  $\sim 10^{16}$ – $10^{17}$  bits to describe the intergalactic medium at  $\sim 100$  kpc resolution. The multifractal geometry of galaxy clustering, described by the generalized fractal dimension  $D_q$  and the singularity spectrum  $g(\alpha)$ , has been measured from galaxy surveys and  $N$ -body simulations [14], and Fisher information applied to tidal-web power spectra has been shown to improve neutrino mass constraints by a factor of the order of 15 over density-only analyses [15].

The present work extends these efforts in four directions. We derive the Shannon entropy of the *tidal eigenvalue distribution* analytically from the Doroshkevich PDF, separating it into an isotropic (density) part and an anisotropy term encoding eigenvalue spread. We prove that the traceless shear tensor  $\mathbf{T}$  carries five times the differential entropy of  $\delta$  in the linear Gaussian field, so that density-only analyses discard  $\sim 83\%$  of the available tidal information. We connect the information dimension  $D_1$  — the  $q \rightarrow 1$  Rényi limit — explicitly to the rate of growth of the tidal-field Shannon entropy with resolution, bridging the multifractal and information-theoretic descriptions. Finally, we compute the redshift evolution of the multifractal entropy and derive its relation to the

linear growth rate  $f(z)$ , providing an independent constraint complementary to redshift-space-distortion measurements of  $f\sigma_8$ .

### Information Theory

Information theory offers a complementary, basis-independent approach. The Shannon entropy [16]

$$H = - \sum_i p_i \log_2 p_i \quad (\text{bits}) \quad (1)$$

quantifies the uncertainty—or information content—of a probability distribution  $\{p_i\}$ . For a *continuous* random variable  $\rho$ , such as a tidal eigenvalue or a shear invariant, the differential (continuous) Shannon entropy generalizes Eq. (1) to

$$h[\rho] = - \int \mathcal{P}(\rho) \log \mathcal{P}(\rho) d\rho \quad (2)$$

Unlike  $H$ , the differential entropy  $h$  is not invariant under nonlinear reparametrizations, but differences of differential entropies and mutual information are invariant [17].

Furthermore, the fractal geometry of the Cosmic Web introduces another layer of information: each morphological component is characterized by a Hausdorff dimension  $D_H < 3$  [18, 19], and the full multifractal spectrum  $g(\alpha)$  encodes how the singularity strengths of the density field are distributed across scales. The generalized Rényi dimensions  $D_q$  interpolate between the Hausdorff dimension ( $q \rightarrow 0$ ), the information dimension ( $q \rightarrow 1$ ), and the correlation dimension ( $q \rightarrow 2$ ), providing a hierarchy of information measures that bridges geometry and statistics.

In the following sections we carry out this programme for the tidal eigenvalue distribution, the shear invariants, the multifractal spectrum, and their joint redshift evolution.

## II. TIDAL DEFORMATION TENSOR AND MORPHOLOGICAL CLASSIFICATION

The gravitational tidal tensor is the Hessian of the peculiar gravitational potential  $\phi$  (related to  $\delta$  by the Poisson equation  $\nabla^2 \phi = 4\pi G \bar{\rho} a^2 \delta$  in comoving coordinates):

$$\Psi_{ij}(\mathbf{q}) = \frac{\partial^2 \phi}{\partial q_i \partial q_j}. \quad (3)$$

In linear theory  $\Psi_{ij}$  coincides (up to a sign convention) with the deformation tensor of Lagrangian perturbation theory. Let  $\lambda_1 \geq \lambda_2 \geq \lambda_3$  be the ordered eigenvalues of  $\Psi_{ij}$ . By the Poisson equation,

$$\delta = \text{Tr}(\Psi) = \lambda_1 + \lambda_2 + \lambda_3. \quad (4)$$

### T-web classification

Following the T-web formalism of Hahn et al. [4], a point in the density field is classified by the number  $n_+$  of *positive* eigenvalues, relative to a threshold  $\lambda_{\text{th}} \geq 0$ :

$$\text{web type} = \begin{cases} \text{cluster} & n_+ = 3, \\ \text{filament} & n_+ = 2, \\ \text{wall} & n_+ = 1, \\ \text{void} & n_+ = 0. \end{cases} \quad (5)$$

Each configuration corresponds to collapse along 3, 2, 1, or 0 principal axes, respectively, in the Zel'dovich approximation. The threshold  $\lambda_{\text{th}}$  is a free parameter;  $\lambda_{\text{th}} = 0$  is the standard choice in the linear regime.

### Independent shear invariants

The three scalar invariants of  $\Psi_{ij}$  are

$$I_1 = \text{Tr}(\Psi) = \lambda_1 + \lambda_2 + \lambda_3, \quad (6)$$

$$I_2 = \frac{1}{2} [(\text{Tr} \Psi)^2 - \text{Tr}(\Psi^2)] = \lambda_1 \lambda_2 + \lambda_1 \lambda_3 + \lambda_2 \lambda_3, \quad (7)$$

$$I_3 = \det(\Psi) = \lambda_1 \lambda_2 \lambda_3. \quad (8)$$

It is, however, more natural for information-theoretic purposes to work with the *traceless* shear tensor

$$T_{ij} = \Psi_{ij} - \frac{\delta}{3} \delta_{ij}^{(K)}, \quad (9)$$

where  $\delta_{ij}^{(K)}$  is the Kronecker delta. The two non-trivial invariants of  $\mathbf{T}$  are

$$\mathcal{Q} \equiv \text{Tr}(\mathbf{T}^2) = \text{Tr}(\Psi^2) - \frac{1}{3} \delta^2, \quad (10)$$

$$\mathcal{A} \equiv \text{Tr}(\mathbf{T}^3) = \text{Tr}(\Psi^3) - \delta \text{Tr}(\Psi^2) + \frac{2}{9} \delta^3. \quad (11)$$

$\mathcal{Q} \geq 0$  is the squared shear amplitude, vanishing only for perfectly isotropic configurations ( $\lambda_1 = \lambda_2 = \lambda_3$ ).  $\mathcal{A}$  measures the skewness of the eigenvalue distribution and changes sign between prolate and oblate geometries. The triplet  $(\delta, \mathcal{Q}, \mathcal{A})$  uniquely determines the set  $\{\lambda_i\}$  up to permutation; it forms a complete, irreducible basis for the information content of  $\Psi_{ij}$ .

## III. ENTROPY OF THE TIDAL EIGENVALUE DISTRIBUTION

In the linear regime, when the density perturbations form a Gaussian random field, the joint PDF of the three ordered eigenvalues  $\lambda_1 \geq \lambda_2 \geq \lambda_3$  of the tidal Hessian was derived by Doroshkevich [20, 21] (see Appendix):

$$\mathcal{P}(\lambda_1, \lambda_2, \lambda_3) = \frac{\Delta}{8\pi\sqrt{5}\sigma_\lambda^6} \exp\left(-\frac{6I_1^2 - 15I_2}{2\sigma_\lambda^2}\right), \quad (12)$$

where  $\Delta \equiv (\lambda_1 - \lambda_2)(\lambda_2 - \lambda_3)(\lambda_1 - \lambda_3)$  is the eigenvalue spread, defined on the domain  $\lambda_1 \geq \lambda_2 \geq \lambda_3$ ; where  $\sigma_\lambda^2 = \sigma_\delta^2/15$  is the one-dimensional eigenvalue variance, and  $\sigma_\delta^2$  is the linear density variance smoothed on a given scale [22]. The Vandermonde-like factor  $\Delta$  enforces the ordering and suppresses configurations with degenerate eigenvalues, reflecting the tendency of tidal fields to favor *triaxial* rather than isotropic geometries. The Doroshkevich distribution can then be written as

$$\mathcal{P}(u, v) = \mathcal{N} v^{3/2} \exp\left(-\frac{5v}{2\sigma_\delta^2} - \frac{u^2}{2\sigma_\delta^2}\right), \quad (13)$$

in terms of independent variables  $u = I_1 \in (-\infty, \infty)$  and  $v = I_1^2 - 3I_2 \in (0, \infty)$ , as derived in the Appendix.

The marginal PDF of each eigenvalue and the fraction of volume in each T-web class follow by integration. In particular, the fraction of volume with  $n_+ = k$  positive eigenvalues (at threshold  $\lambda_{\text{th}} = 0$ ) gives the discrete distribution  $\{p_i\}$  used in Eq. (1).

### Differential entropy of the tidal field

The full differential Shannon entropy of the joint eigenvalue distribution is

$$h[\boldsymbol{\lambda}] = - \iiint_{\lambda_1 \geq \lambda_2 \geq \lambda_3} \mathcal{P}(\boldsymbol{\lambda}) \log \mathcal{P}(\boldsymbol{\lambda}) d\lambda_1 d\lambda_2 d\lambda_3. \quad (14)$$

or equivalently

$$h[\mathbf{I}] = - \iint_{I_1^2 \geq 3I_2} \mathcal{P}(I_1, I_2) \log \mathcal{P}(I_1, I_2) dI_1 dI_2. \quad (15)$$

Substituting Eq. (13) and separating the Gaussian and Vandermonde contributions:

$$h[\mathbf{I}] = \log\left(8\pi\sqrt{5}\sigma_\lambda^6\right) + 3 - \frac{3}{2} \langle \log v \rangle, \quad (16)$$

where  $\langle \cdot \rangle$  denotes averaging over  $\mathcal{P}(u, v)$ . The first two terms are determined by  $\sigma_\lambda$  alone; the third encodes the information in the *anisotropy* of the eigenvalue spectrum. Using the moments of the Doroshkevich distribution [23], one obtains

$$h[\mathbf{I}] = \log\left(\frac{8\pi\sqrt{5}\sigma_\lambda^6}{e}\right) + \frac{3}{2}\gamma - \frac{3}{2} \log\left(\frac{3}{2}\sigma_\lambda^2\right), \quad (17)$$

where  $\gamma = 0.5772\dots$  is the Euler constant. The term  $-\langle \log v \rangle > 0$  is positive definite and represents the information *lost* due to the ordering constraint; it increases with the anisotropy of the tidal field and is minimized in isotropic configurations ( $\Delta \rightarrow 0$  or  $I_1^2 \rightarrow 3I_2$ ), where the distribution concentrates on the constraint surface.

### Entropy of the shear invariants

Since  $(\delta, \mathcal{Q}, \mathcal{A})$  constitute a change of variables from  $(\lambda_1, \lambda_2, \lambda_3)$ , the information content is conserved up to the Jacobian. In the Gaussian linear field,  $\delta$  and  $\mathcal{Q}$  are *statistically independent* [24]: the isotropic part (density) decouples from the anisotropic part (shear). Consequently, the entropy decomposes as

$$h[\boldsymbol{\lambda}] = h[\delta] + h[\mathcal{Q}, \mathcal{A}] + \text{const}, \quad (18)$$

where the constant accounts for the Jacobian of the transformation. The differential entropy of the density contrast alone is that of a Gaussian:

$$h[\delta] = \frac{1}{2} \log(2\pi e \sigma_\delta^2). \quad (19)$$

The additional entropy residing in  $(\mathcal{Q}, \mathcal{A})$  therefore captures *geometric* information about anisotropic collapse that is invisible to density-field statistics. In practice,  $\mathcal{Q}$  follows a scaled chi-squared distribution (it is a sum of squares of five Gaussian variates in the irreducible representation of the shear), while the joint distribution of  $(\mathcal{Q}, \mathcal{A})$  is related to that of a  $3 \times 3$  Gaussian orthogonal ensemble [25].

The mutual information between  $\delta$  and the morphological class (T-web label) is

$$\mathcal{I}(\delta; \text{web}) = H(\text{web}) - H(\text{web}|\delta), \quad (20)$$

where  $H(\text{web}) = 1.70$  bits (Table I) and  $H(\text{web}|\delta)$  is the conditional entropy of the morphological label given the local density. Because two regions with the same  $\delta$  can have different  $(\mathcal{Q}, \mathcal{A})$  and hence different T-web types, we have  $H(\text{web}|\delta) > 0$ : the shear invariants carry information about morphology that is not captured by the density alone.

## IV. FRACTAL GEOMETRY AND MULTIFRACTAL ENTROPY

### Hausdorff dimensions of Cosmic Web components

The Cosmic Web is not space-filling: each morphological component occupies a set of non-integer Hausdorff dimension  $D_H < 3$  [18]. Measurements from  $N$ -body simulations and galaxy surveys [19, 26] yield the approximate values

$$D_H \approx \begin{cases} 1.2\text{--}1.5 & \text{clusters (nodes),} \\ 1.7\text{--}1.9 & \text{filaments,} \\ 2.4\text{--}2.7 & \text{walls,} \\ 3.0 & \text{voids (fill 3-D volume),} \end{cases} \quad (21)$$

where lower  $D_H$  reflects stronger geometrical compression. Clusters and filaments have the lowest dimensions

because matter is compressed along three and two axes, respectively, while walls are compressed along one axis only.

### Rényi entropy and generalized dimensions

The multifractal formalism [27, 28] generalises the notion of a single fractal dimension to a spectrum of *generalized dimensions*

$$D_q = \frac{1}{q-1} \lim_{\ell \rightarrow 0} \frac{\log \sum_i p_i(\ell)^q}{\log \ell}, \quad q \neq 1, \quad (22)$$

where the sum is over cells of linear size  $\ell$  and  $p_i(\ell)$  is the probability (mass fraction) in cell  $i$ . The  $q = 0$  limit gives the Hausdorff dimension,  $D_0 = D_H$ . The  $q \rightarrow 1$  limit defines the *information dimension*

$$D_1 = \lim_{\ell \rightarrow 0} \frac{-\sum_i p_i(\ell) \log p_i(\ell)}{\log(1/\ell)} = \lim_{\ell \rightarrow 0} \frac{H(\ell)}{\log(1/\ell)}, \quad (23)$$

which is precisely the rate at which the Shannon entropy  $H(\ell)$  of the density field grows as the resolution scale  $\ell$  decreases. The  $q = 2$  limit gives the correlation dimension  $D_2$ , related to the two-point correlation function of the density contrast,  $\xi(r) \sim r^{-(3-D_2)}$  [19, 29].

The generalized dimensions satisfy  $D_0 \geq D_1 \geq D_2 \geq \dots$ , with equality holding only for a monofractal (uniform mass distribution on a single fractal set). The degree of multifractality is quantified by the *width* of the singularity spectrum  $g(\alpha)$ , which is the Legendre transform of  $(q-1)D_q$ :

$$g(\alpha) = q\alpha - (q-1)D_q, \quad \alpha = \frac{d[(q-1)D_q]}{dq}. \quad (24)$$

Here  $\alpha$  is the local Hölder (Lipschitz) exponent of the density measure, and  $g(\alpha)$  is the Hausdorff dimension of the set of points with that exponent. The peak of  $g(\alpha)$  at  $\alpha = D_1$  corresponds to the dominant singularity strength, and the width  $\Delta\alpha = \alpha_{\max} - \alpha_{\min}$  measures the heterogeneity of the fractal.

### Entropy growth rate and information dimension

Combining Eqs. (23) and (1), the information dimension of a given web component  $i = \{\text{voids, walls, filaments, clusters}\}$  is

$$D_1^{(i)} = \lim_{\ell \rightarrow 0} \frac{H^{(i)}(\ell)}{\log(1/\ell)}, \quad (25)$$

where  $H^{(i)}(\ell)$  is the Shannon entropy of the mass distribution *within* component  $i$  at resolution  $\ell$ . For a uniform distribution on a  $D_H$ -dimensional fractal,  $H^{(i)}(\ell) \approx D_H \log(1/\ell)$  and hence  $D_1^{(i)} = D_H^{(i)}$ . Departures from

this monofractal scaling—measured by  $D_0 - D_1 > 0$ —quantify the excess information due to the heterogeneous, multifractal distribution of matter within each component.

For filaments, the relatively low  $D_H \approx 1.8$  combined with the large mass fraction  $p_F \approx 0.4$  implies a high *information density per unit volume*: the filament network packs a disproportionate amount of Shannon entropy into a small fraction of the cosmic volume. This is the geometric analogue of the maximum entropy result of Section V.

## V. ENTROPY BUDGET OF THE COSMIC WEB

### Discrete entropy of morphological components

Table I summarizes the volume and mass filling fractions of the four T-web components, together with their contributions to the discrete Shannon entropy  $H^{(M)}$  of the matter distribution.

TABLE I. Volume and mass filling fractions of Cosmic Web components, their density contrast range, Hausdorff dimension, information and entropy contributions. Filling fractions from Refs. [30–32]; fractal dimension from Refs. [19, 30].

Type	$p_i^{(V)}$	$p_i^{(M)}$	$\delta$ range	$D_H$	$-p_i^{(M)} \log_2 p_i^{(M)}$
Voids	0.77	0.03	$< -0.8$	3.0	0.152
Walls	0.16	0.33	0–5	2.5	0.528
Filaments	0.06	0.40	5–50	1.8	0.529
Clusters	0.01	0.24	$> 100$	1.2	0.494

Summing the different contributions:

$$H^{(V)} = 1.03 \text{ bits}, \quad (26)$$

$$H^{(M)} = 1.70 \text{ bits}. \quad (27)$$

The maximum possible entropy for a 4-component system is  $H_{\max} = \log_2 4 = 2$  bits, achieved when all components carry equal mass. The Cosmic Web thus operates at  $\sim 85\%$  of the maximum information capacity.

### Dominant contribution from filaments

The entropy function  $f(p) = -p \log_2 p$  attains its global maximum at  $p^* = e^{-1} \approx 0.368$ , with  $f(p^*) = (\log_2 e) e^{-1} \approx 0.531$  bits. The matter fraction of filaments and walls place them near this maximum. Consequently, *filaments and walls carry the maximum possible per-component entropy* for their matter fraction, and dominate the total  $H^{(M)}$ , see Fig.1.

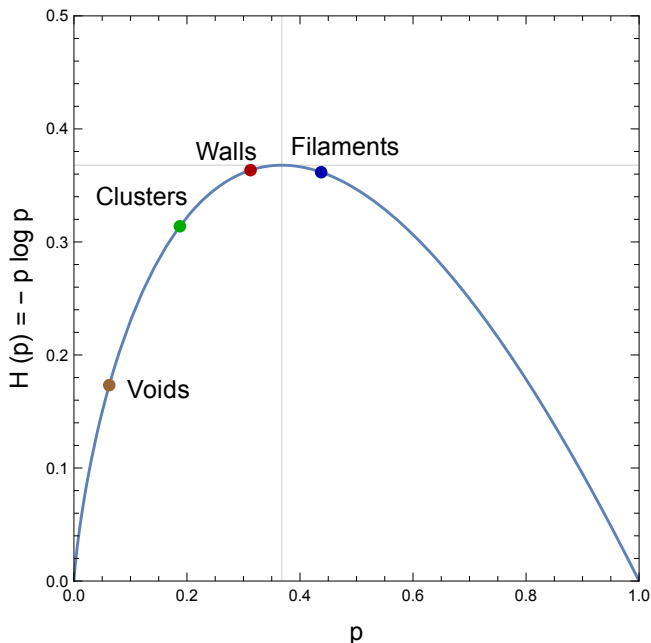


FIG. 1. The function  $H(p) = -p \log p$  peaks at  $p = 1/e \approx 0.37$ . Filaments and Walls hold  $\sim 40\%$  and  $33\%$  of cosmic matter, respectively — placing them near the theoretical maximum. On the other hand, voids and clusters are on the low-entropy tails: too rare or too dominant.

### The entropy in shear invariants

Since the morphological label is not determined by  $\delta$  alone, the shear invariants  $\mathcal{Q}$  and  $\mathcal{A}$  carry additional, statistically independent information. The mutual information between  $(\mathcal{Q}, \mathcal{A})$  and the T-web morphological class,

$$\mathcal{I}(\mathcal{Q}, \mathcal{A}; \text{web}) = H(\text{web}) - H(\text{web}|\mathcal{Q}, \mathcal{A}), \quad (28)$$

quantifies how much of the morphological entropy is resolved by the shear. In the Doroshkevich model, the five independent components of the traceless shear tensor  $\mathbf{T}$  each contribute  $\frac{1}{2} \log(2\pi e \sigma_T^2)$  bits of differential entropy, where  $\sigma_T^2 = \frac{2}{15} \sigma_\delta^2$ , yielding a total shear entropy of

$$h[\mathbf{T}] = \frac{5}{2} \log(2\pi e \sigma_T^2) \simeq \frac{5}{2} \log(2\pi e \sigma_\delta^2) - 5. \quad (29)$$

This exceeds  $h[\delta]$  by about a factor five, confirming that the tidal field carries substantially more morphological information than the density contrast alone.

### Log-normal approximation in the mildly nonlinear regime

In the mildly nonlinear regime, the cosmic density PDF is well approximated by a log-normal distribution [33]:

$$\mathcal{P}(\delta) = \frac{1}{\sqrt{2\pi} \sigma_{\ln}(1+\delta)} \exp\left[-\frac{(\ln(1+\delta) - \mu)^2}{2\sigma_{\ln}^2}\right], \quad (30)$$

with differential entropy

$$h[\delta] = \frac{1}{2} \log(2\pi e \sigma_{\ln}^2) + \mu + \frac{1}{2} \sigma_{\ln}^2. \quad (31)$$

The peak entropy contribution per volume element occurs at  $1 + \delta = e^{\mu - \sigma_{\ln}^2}$ , which for typical  $\Lambda$ CDM parameters at  $z = 0$  ( $\mu \approx -\sigma_{\ln}^2/2$ ,  $\sigma_{\ln}^2 \approx 0.8$ ) gives  $1 + \delta_{\text{peak}} \approx e^{-\sigma_{\ln}^2/2} \approx 0.67$ , corresponding to mildly underdense regions at the void-wall boundary [34–36]. Crucially, this is distinct from the *mass-weighted* entropy maximum, which selects the filament regime: the two measures resolve complementary aspects of the density field.

## VI. REDSHIFT EVOLUTION OF ENTROPY

At high redshift the matter distribution approaches uniformity:  $p_i^{(M)} \rightarrow 1/4$  and  $H^{(M)} \rightarrow 2$  bits. As gravitational clustering proceeds, matter evacuates voids, enriches filaments, and concentrates in clusters, shifting the distribution away from uniformity and *decreasing* the Shannon entropy in configuration space. The growth of the Cosmic Web is thus an entropy-decreasing process in configuration space — an instance of gravitational self-organization far from thermodynamic equilibrium [26] (see also the Note Added for the complementary phase-space perspective).

Concurrently, the information dimension of each component evolves: at high  $z$  the matter field is nearly Gaussian and monofractal ( $D_0 \approx D_1 \approx D_2 \approx 3$ ), while at low  $z$  the multifractal spectrum broadens, with  $\Delta\alpha = \alpha_{\text{max}} - \alpha_{\text{min}}$  growing as voids become emptier and clusters denser. The *multifractal entropy rate*

$$\dot{H}_{\text{mf}}(z) \equiv \frac{d}{dz} [D_1(z) \log(1/\ell)] \quad (32)$$

provides a redshift-dependent measure of the rate at which structural information is generated by gravitational collapse. We now derive this rate analytically in terms of the linear growth factor  $D(z)$  and the growth rate  $f(a)$ .

Let us consider a simple Ansatz for the evolution of the probability of cosmic matter in the four component (filaments, walls, clusters and voids) cosmic web:  $p_i(\alpha) = 1/4 + \alpha(2i - 5)/2$  such that  $\sum_i p_i(\alpha) = 1, \forall \alpha$ . The Shannon entropy then becomes

$$\begin{aligned} H(\alpha) &= -\sum_i p_i(\alpha) \log p_i(\alpha) \\ &= 2 - \frac{1}{4} \log [(1 - 2\alpha)^{1-2\alpha} (1 - 2\alpha)^{1+2\alpha}] \\ &\quad - \frac{1}{4} \log [(1 - 6\alpha)^{1-6\alpha} (1 + 6\alpha)^{1+6\alpha}]. \end{aligned} \quad (33)$$

Cosmic evolution starts at high redshift with  $\alpha \rightarrow 0$  and all components equally distributed,  $p_i = 1/4$ , and thus

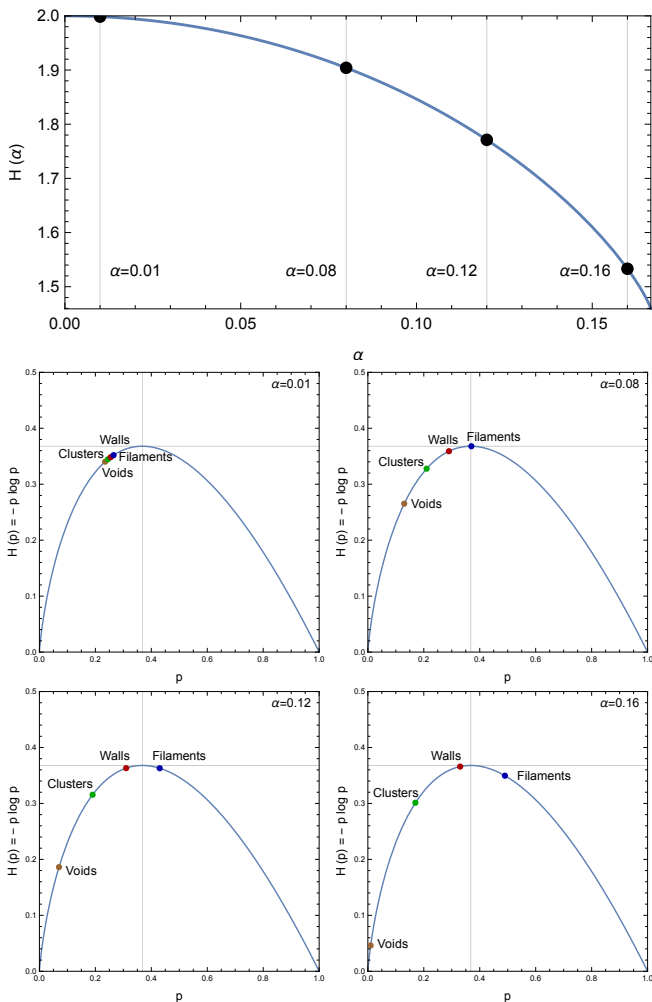


FIG. 2. *Top panel:* The function  $H(\alpha)$  in Eq. (33) as a function of the divergence  $\alpha$ . *Bottom panels:* The location of the Cosmic Web components as we move from  $\alpha \simeq 0$  at high redshift to  $\alpha \simeq 1/6$ . It is clear that, as time progresses ( $\alpha$  grows), the Cosmic Web becomes more complex (structured) and the Shannon entropy  $H(\alpha)$  reduces well below the maximum. Note that filaments soon become the dominant component and remain so until quite late, while clusters and walls do not change much over time, and voids very quickly become irrelevant to the total Shannon entropy.

$H(0) = H_{\max} = 2$ . As time progresses, alpha grows and the different components' mass probabilities start to diverge from each other, while the comic web develops. The Shannon entropy decreases following Eq. (33), see Fig. 2.

### Growth factor and tidal eigenvalue variance

The linear density variance smoothed on scale  $R$  evolves as

$$\sigma_\delta^2(R, z) = D(z)^2 \sigma_\delta^2(R, 0), \quad (34)$$

where  $D(z) \equiv D(a)/D(a_0)$  is the linear growth factor normalized to unity at  $z = 0$ , which satisfies the growth equation

$$\ddot{D} + 2H(z)\dot{D} = \frac{3}{2}\Omega_{m,0}H_0^2(1+z)^3D, \quad (35)$$

with  $H(z) = H_0E(z)$ ,  $E^2(z) = \Omega_{m,0}(1+z)^3 + \Omega_\Lambda$ . Since  $\sigma_\lambda^2 = \sigma_\delta^2/15$ , see Eq. (70), the eigenvalue variance scales identically:

$$\sigma_\lambda(z) = \sigma_\lambda(0)D(z). \quad (36)$$

The *growth rate* is defined as the logarithmic derivative of  $D$  with respect to the scale factor  $a = (1+z)^{-1}$ ,

$$f(a) \equiv \frac{d \ln D}{d \ln a}, \quad (37)$$

which, in the Linder [37] approximation, is well-fitted by

$$f(z) \approx \Omega_m(z)^\gamma, \quad \gamma \simeq 0.55, \quad (38)$$

where  $\Omega_m(z) = \Omega_{m,0}(1+z)^3/E^2(z)$ . In a flat  $\Lambda$ CDM universe with  $\Omega_{m,0} = 0.3$ ,  $f(0) \approx 0.52$  and  $f \rightarrow 1$  as  $z \rightarrow \infty$  (matter domination, Einstein-de Sitter limit).

### Redshift evolution of the differential entropy

Substituting Eq. (36) into Eq. (17), the tidal eigenvalue entropy acquires an explicit redshift dependence:

$$h[\mathbf{I}](z) = h[\mathbf{I}](0) + 3 \ln D(z), \quad (39)$$

where  $h[\mathbf{I}](0) = \ln(8\pi\sqrt{5}\sigma_\lambda^6(0)/e) + 3/2(\gamma - \ln(3\sigma_\lambda^2(0)/2))$  is the present-day value and all logarithms are natural. This compact result follows directly from the  $\sigma_\lambda^6/\sigma_\lambda^3 = \sigma_\lambda^3$  dependence in Eq. (17). The analogous expressions for the density and shear entropies are

$$h[\delta](z) = h[\delta](0) + \ln D(z), \quad (40)$$

$$h[\mathbf{T}](z) = h[\mathbf{T}](0) + 5 \ln D(z), \quad (41)$$

confirming that the 5:1 ratio  $h[\mathbf{T}] \simeq 5h[\delta]$  is *preserved at all redshifts* in linear theory, since both sides shift by the same number of  $\ln D$  factors up to an integer multiple. As  $z \rightarrow \infty$ ,  $D(z) \rightarrow 0$  and all three entropies diverge to  $-\infty$ , reflecting the approach to perfect Gaussianity and spatial uniformity (maximum discrete entropy  $H^{(M)} \rightarrow 2$  bits, minimum differential entropy).

Differentiating Eq. (39) with respect to  $z$  and using  $d \ln D/dz = -f(z)/(1+z)$ , from Eq. (37):

$$\frac{dh[\mathbf{I}]}{dz} = -\frac{3f(z)}{1+z} = 3 \frac{d \ln D}{dz}. \quad (42)$$

This is positive (entropy increasing with  $z$ , i.e. toward the past) at all epochs, as required by the approach to uniformity. In the Einstein-de Sitter limit ( $f \rightarrow 1$ ,  $D \propto (1+z)^{-1}$ ), the rate simplifies to  $dh/dz = 3/(1+z)$ , integrating to  $h(z) - h(0) = 3 \ln(1+z)$  — a pure logarithmic growth in volume with redshift.

### Master relation: entropy rate and growth rate

Substituting Eq. (36) into the definition Eq. (32) and using  $D_1(z) \propto h[\mathbf{I}](z)/\log(1/\ell)$  from Eq. (23) gives

$$\dot{H}_{\text{mf}}(z) = \frac{d}{dz} [D_1(z) \log(1/\ell)] = -\frac{3f(z)}{1+z} = 3 \frac{d \ln D}{dz}. \quad (43)$$

This result has three immediate consequences:

- *Scale independence.* The factor  $\log(1/\ell)$  cancels exactly:  $\dot{H}_{\text{mf}}$  is independent of the smoothing scale  $\ell$ . The entropy rate is a purely cosmological quantity, carrying no dependence on the resolution at which the field is probed.

- *Direct measurement of  $f(z)$ .* Equation (43) implies

$$f(z) = -\frac{(1+z)}{3} \dot{H}_{\text{mf}}(z), \quad (44)$$

so that the growth rate — the primary discriminator between general relativity and modified-gravity theories [37] — can be read off directly from the time derivative of the tidal Shannon entropy. Combined with Eq. (38), a measurement of  $\dot{H}_{\text{mf}}$  at a single redshift determines  $\Omega_m(z)$ , and its evolution tests the  $\gamma \simeq 0.55$  prediction of GR.

- *Connection with  $D(z)$  and  $\sigma_8$ .* Integrating Eq. (43) between two redshifts  $z_1 < z_2$ ,

$$h[\mathbf{I}](z_1) - h[\mathbf{I}](z_2) = 3 \ln \frac{D(z_1)}{D(z_2)}, \quad (45)$$

so the *ratio of growth factors* at two epochs is directly exponential in the entropy difference:

$$\frac{D(z_1)}{D(z_2)} = \exp \left[ \frac{h[\mathbf{I}](z_1) - h[\mathbf{I}](z_2)}{3} \right]. \quad (46)$$

In practice,  $h[\mathbf{I}](z) = \text{const} + \ln \sigma_8^2(z)$ , so this reduces to  $D(z_1)/D(z_2) = \sigma_8(z_1)/\sigma_8(z_2)$ , which is the standard growth-factor estimator — but here derived as a consequence of the information-theoretic approach. At fixed smoothing scale  $R = 8 h^{-1} \text{Mpc}$ ,  $\sigma_8(z) = \sigma_8 D(z)$ , giving

$$h[\mathbf{I}](z) = h[\mathbf{I}](0) + 3 \ln[\sigma_8 D(z)/\sigma_8] \quad (47)$$

$$= h[\mathbf{I}](0) + 3 \ln D(z). \quad (48)$$

The present-day entropy  $h[\mathbf{I}](0)$  is therefore directly sensitive to  $\sigma_8$ : a 1% measurement of  $h$  implies a 0.5% constraint on  $\sigma_8 D(z)$ , competitive with standard power-spectrum analyses but using a single scalar statistic.

### Information dimension and the growth rate

Equation (43) also constrains the redshift evolution of the information dimension  $D_1(z)$  introduced in Eq. (23). From  $H_{\text{mf}} = D_1(z) \log(1/\ell)$  and Eq. (43):

$$\frac{dD_1}{dz} = -\frac{3f(z)}{(1+z) \log(1/\ell)}, \quad (49)$$

which integrates to

$$D_1(z) = D_1(0) + \frac{3 \ln D(z)}{\log(1/\ell)}. \quad (50)$$

Since  $\ln D(z) < 0$  for all  $z > 0$  (with  $D(0) = 1$ ), the information dimension *decreases* from its high- $z$  value of  $D_1 \approx 3$  (near-Gaussian monofractal) toward its present-day value  $D_1(0) < 3$ . The deficit  $D_0 - D_1(z)$ , which quantifies the degree of multifractality (Section IV.C), therefore grows as

$$\frac{d}{dz} [D_0 - D_1(z)] = \frac{3f(z)}{(1+z) \log(1/\ell)} > 0, \quad (51)$$

confirming that the multifractal character of the mass distribution *increases monotonically* as structure forms. The rate is faster (larger  $f$ ) in epochs of rapid structure growth, and slower in dark-energy dominated epochs where  $f$  is suppressed.

The width of the singularity spectrum  $\Delta\alpha(z)$  is related to  $D_0 - D_1$  by the convexity of  $g(\alpha)$ , and its growth rate satisfies

$$\frac{d\Delta\alpha}{dz} \propto \frac{d(D_0 - D_1)}{dz} = \frac{3f(z)}{(1+z) \log(1/\ell)}, \quad (52)$$

where the proportionality constant depends on the shape of  $g(\alpha)$  and hence on the cosmological model. Measuring  $\Delta\alpha(z)$  from simulations or survey data at multiple redshifts therefore provides an independent constraint on  $f(z)$ , complementary to standard redshift-space-distortion measurements of  $f\sigma_8$ .

Fig. 3 shows the redshift dependence of the key entropy quantities for a flat  $\Lambda$ CDM cosmology with  $\Omega_{m,0} = 0.3$ ,  $\sigma_8 = 0.8$ . It also shows that  $\dot{H}_{\text{mf}}$  is largest in magnitude at low redshift where structure formation is suppressed by dark energy: the transition from matter domination to  $\Lambda$  domination at  $z \approx 0.3$  marks an inflection point in the entropy curve where  $\dot{H}_{\text{mf}}$  changes sign. At high redshift  $\dot{H}_{\text{mf}} \rightarrow -3/(1+z)$  (EdS limit,  $f \rightarrow 1$ ), so the entropy evolves logarithmically:  $h(z) \rightarrow h(0) + 3 \ln(1+z)$ . The ratio  $|\dot{H}_{\text{mf}}(z)(1+z)| = 3f(z)$  provides a direct, epoch-by-epoch measure of the growth rate, offering a summary statistic for next-generation surveys.

## VII. DISCUSSION

Three distinct information measures characterise the Cosmic Web at different levels of description: the discrete Shannon entropy of the T-web morphological classification, the continuous differential entropy of the tidal eigenvalue distribution, and the multifractal information dimension. Each probes a complementary aspect of the total information budget, and together paint a richer statistical picture of large-scale structure than the density contrast alone.

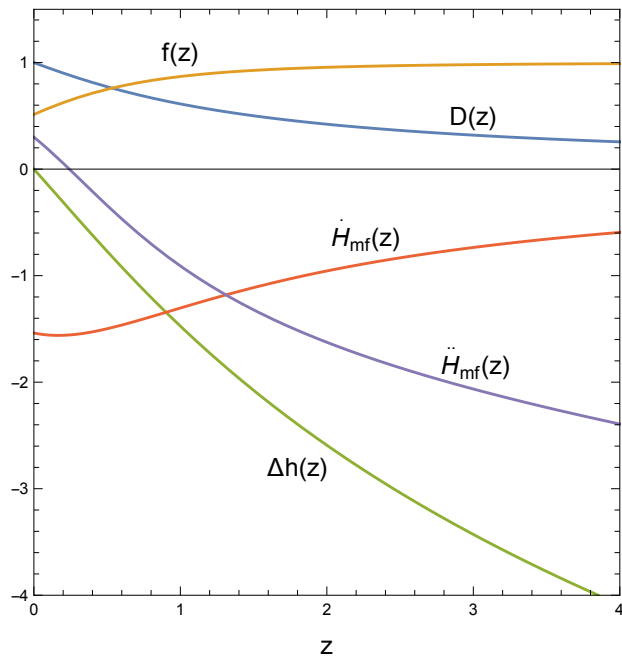


FIG. 3. Redshift evolution of the growth factor  $D(z)$ , growth rate  $f(z)$ , differential entropy shift  $\Delta h \equiv h(z) - h(0)$  (in nats), and the multifractal entropy rate  $\dot{H}_{\text{mf}}(z)$  (in nats per unit redshift), for flat  $\Lambda$ CDM with  $\Omega_{m,0} = 0.3$  and  $\sigma_8 = 0.8$ . At  $z = 0$ :  $h(0) = \ln(8\pi\sqrt{5}\sigma_\lambda^6/e) + 3/2(\gamma - \ln(3\sigma_\lambda^2/2))$ .

*Tidal entropy as a cosmological probe.* The differential entropy  $h[\boldsymbol{\lambda}]$  in Eq. (17) depends on  $\sigma_\lambda \propto \sigma_\delta$ , which in turn depends on the matter power spectrum  $P(k)$  and the growth factor  $D(z)$ . Measuring  $h[\boldsymbol{\lambda}]$  from reconstructed tidal fields in galaxy surveys therefore provides a single-number summary statistic sensitive to the shape of  $P(k)$  and the growth of structure. It complements both the standard two-point statistics [38, 39] and the Fisher-information approach of Bonnaire et al. [15], who demonstrated that environment-split power spectra improve neutrino mass constraints by a factor of  $\sim 15$  over the matter power spectrum alone, and the classifier-comparison framework of Leclercq et al. [9], which used the Jensen–Shannon divergence to rank T-web, DIVA and ORIGAMI [10] classifiers for parameter inference.

*Shear information beyond density.* The fact that  $h[\mathbf{T}] = 5h[\delta]$  at linear order (from the 5:1 component ratio of the shear tensor) implies that density-field analyses discard approximately  $5/6 \approx 83\%$  of the linear information available in the tidal tensor. Field-level inference methods that reconstruct the full  $\Psi_{ij}$  [39, 40] recover this information, but current summary statistics based on  $\delta$  alone do not.

*Multifractal discriminators.* The generalized dimension spectrum  $D_q$  and the singularity spectrum  $g(\alpha)$  are sensitive to the non-Gaussianity generated by gravitational collapse and to the cosmological model. Gaite [14] showed that a nonlacunar multifractal geometry with

$\alpha_{\text{min}} \approx 1$  simultaneously describes web structure, hierarchical clustering, and halo distributions in SDSS and  $N$ -body simulations; this connects that observed spectrum explicitly to the Shannon information dimension  $D_1$ . Modified gravity theories that alter the growth rate  $f\sigma_8$  also alter the width  $\Delta\alpha$  of the multifractal spectrum. Measuring  $D_q$  for  $q = 0, 1, 2$  from galaxy catalogues provides three complementary constraints beyond the power spectrum.

*Continuous entropy and prior work.* The differential Shannon entropy of the full density field, Eq. (2), could be estimated directly from galaxy surveys via field-level inference [38, 39], bypassing the four-bin discretization of the T-web classification. This complements the Kullback–Leibler entropy of Hosoya et al. [6], which measures *relative* information with respect to a homogeneous reference state, and the Shannon-entropy homogeneity tests of Pandey [8]. The complementary perspective of Vazza [12, 13]—estimating the algorithmic complexity of cosmological simulation outputs at fixed resolution—provides an upper bound on the information content of the cosmic gas field that is independent of the analytical PDF approach pursued here.

## VIII. CONCLUSIONS

We have presented an analytical information-theoretic treatment of the Cosmic Web incorporating the tidal deformation tensor, the shear invariants, and the fractal geometry of large-scale structure. Our main results are:

- *Tidal eigenvalue entropy.* The Doroshkevich PDF yields a closed-form expression for the differential Shannon entropy of  $(\lambda_1, \lambda_2, \lambda_3)$ , Eq. (17), decomposing it into a Gaussian part controlled by  $\sigma_\delta$  and an anisotropy term  $-\langle \log \Delta \rangle$  encoding the eigenvalue spread. The traceless shear tensor  $\mathbf{T}$  carries five degrees of freedom, giving a differential entropy that exceeds  $h[\delta]$  by a factor of five; the invariants  $\mathcal{Q}$  and  $\mathcal{A}$  are statistically independent of  $\delta$  and resolve morphological information invisible to the density alone.

- *Entropy budget.* The discrete matter-weighted entropy is  $H^{(M)} \approx 1.70$  bits ( $\sim 85\%$  of the maximum), with filaments and walls each contributing  $\approx 0.53$  bits. Their matter fractions  $p \approx 0.4$  and  $0.33$ , respectively place them near the theoretical maximum of  $-p \log p$  at  $p^* = e^{-1}$ . The low Hausdorff dimension of filaments ( $D_H \approx 1.8$ ) implies the highest information density per unit volume of any web component.

- *Multifractal information dimension.* Each web component is characterized by a spectrum of Rényi dimensions  $D_q$ . The information dimension  $D_1 \leq D_0 = D_H$  measures the rate of Shannon entropy growth with resolution  $\ell$ ; the deficit  $D_0 - D_1$  quantifies multifractality and increases monotonically as structure forms.

- *Redshift evolution and linear growth rate.* The mul-

tifractal entropy rate obeys  $\dot{H}_{\text{mf}}(z) = -3f(z)/(1+z)$ , directly equating the information-theoretic entropy rate to the linear growth rate, independently of smoothing scale. Measuring  $\dot{H}_{\text{mf}}$  at multiple epochs constrains  $f(z)$  and hence tests deviations from general relativity, providing a new statistic, complementary to redshift-space distortion measurements of  $f\sigma_8$ .

- *Shannon entropy and  $\sigma_8$* . The ratio of growth factors between two epochs satisfies  $D(z_1)/D(z_2) = \exp[(h(z_1) - h(z_2))/3]$ , so the tidal Shannon entropy at fixed smoothing scale  $R = 8h^{-1}\text{Mpc}$  directly constrains  $\sigma_8 D(z)$  at the 0.5% level for a 1% entropy measurement.

The principal observational implication is that field-level reconstructions simultaneously inferring  $\delta$  and the full tidal tensor  $\Psi_{ij}$  from surveys such as DESI [41], Euclid [42], and the Vera C. Rubin Observatory [43] would recover the  $\sim 83\%$  of linear tidal information discarded by density-only analyses. Graph-entropy measures of web connectivity [11] and the algorithmic-complexity estimates of Vazza [12, 13] provide independent, resolution-based bounds on the information content that will sharpen as simulation resolution improves.

#### NOTE ADDED

After completion of this work, Kitaura [44] posted a paper entitled *Emergence of Complex Structures* that addresses a closely related set of questions from a substantially different angle. Both papers place the tidal deformation tensor and its eigenvalue spectrum at the centre of the analysis, regard the Gaussian random field as the maximum-entropy baseline from which the Cosmic Web departs under gravitational evolution, and argue that the density contrast  $\delta = \text{Tr } \Psi$  is an incomplete characterization of the available cosmological information. Both also grapple with the same entropy paradox — that structure formation creates geometric order in an evolving Universe — and arrive at consistent resolutions. Kitaura [44] resolves it through the phase-space decomposition  $S_{\text{ps}} = S_x + S_{v|x}$ , where the full phase-space entropy  $S_{\text{ps}}$  increases monotonically while the projected spatial entropy  $S_x \equiv H^{(M)}$  decreases as filaments and clusters form; shell crossing activates velocity degrees of freedom ( $S_{v|x} > 0$ ) that absorb the information shed by the configuration-space field. The present paper arrives at the same conclusion analytically, showing that  $H^{(M)}(z)$  decreases as clustering proceeds.

Kitaura [44] also shows, through a Lagrangian–Eulerian transport analysis, that long-range tidal interaction becomes relevant already at moderate overdensity. This is the dynamical counterpart of the result derived here that the traceless shear tensor  $\mathbf{T}$  carries five times the differential entropy of  $\delta$ : both statements quantify how much morphological information lies beyond the density field, the one through transport geometry and the

other through the Doroshkevich entropy calculus.

The two papers address different regimes and provide different outputs. Kitaura [44] treats the full six-dimensional phase-space dynamics, including shell crossing and multistreaming, and introduces a Landau–Ginzburg free-energy description in which anisotropy acts as an order parameter driving self-organization; this provides the physical mechanism underlying the redshift evolution of  $H^{(M)}$  and the broadening of the singularity spectrum  $g(\alpha)$  described here. He also constructs a hierarchy of deformation tensors beyond the first Hessian, of which the cubic invariant  $\mathcal{A} = \text{Tr}(\mathbf{T}^3)$  of Eq. (11) is the first member. The present paper supplies the analytic entropy calculus in closed form — the Doroshkevich differential entropy, the T-web entropy budget, the factor-of-five shear information advantage, the multifractal  $D_q$  spectrum, and the master relation  $\dot{H}_{\text{mf}} = -2f(z)/(1+z)$  — together with a discussion of observational classifiers not covered in [44].

The two works are consistent and address different aspects of the same underlying physics. Kitaura [44] supplies the dynamical mechanism; this paper supplies the analytic entropy characterization. Read together, they cover the information content of the Cosmic Web from the linear Gaussian regime through the fully nonlinear, multistreaming regime.

#### ACKNOWLEDGMENTS

The author thanks David Alonso and Mikel Martin Barandiaran for stimulating discussions on information theory and large-scale structure. This work was supported by the Research Project PID2024-159420NB-C43 [MICINN-FEDER], and the Centro de Excelencia Severo Ochoa Program CEX2020-001007-S at IFT.

#### APPENDIX: THE DOROSHKEVICH DISTRIBUTION

We derive here the joint probability distribution of the two leading symmetric invariants  $I_1$  and  $I_2$  of the tidal (deformation) tensor for a homogeneous, isotropic Gaussian random field — the result known as the *Doroshkevich distribution* [20, 21]. We then compute the moments  $\langle I_1^2 \rangle$  and  $\langle I_2 \rangle$  analytically, exploiting a remarkable factorization of the distribution that emerges under a natural change of variables. These results underpin the statistical classification of the cosmic web into voids, sheets, filaments, and clusters via the T-web formalism [4].

### Gaussian Random Field and the Tidal Tensor

Let  $\delta(\mathbf{x})$  be a homogeneous, isotropic Gaussian random field representing the cosmological density contrast, smoothed on a scale  $R_s$ . The *tidal tensor* (equivalently, the Hessian of the gravitational potential  $\phi$  through the Poisson equation) is

$$\Psi_{ij}(\mathbf{x}) = \frac{\partial^2 \phi}{\partial x_i \partial x_j}, \quad (53)$$

which is a real, symmetric  $3 \times 3$  matrix with six independent components  $\{\Psi_{11}, \Psi_{22}, \Psi_{33}, \Psi_{12}, \Psi_{13}, \Psi_{23}\}$ .

Because  $\delta$  is Gaussian, these six components are jointly Gaussian with zero mean. Isotropy constrains their covariance tensor completely:

$$\langle \Psi_{ij} \Psi_{kl} \rangle = \frac{\sigma^2}{15} (\delta_{ik} \delta_{jl} + \delta_{il} \delta_{jk} + \delta_{ij} \delta_{kl}), \quad (54)$$

where  $\sigma^2$  is related to the variance of the smoothed density field. From (54) one reads off

$$\langle \Psi_{ii}^2 \rangle = \frac{\sigma^2}{5}, \quad \langle \Psi_{ii} \Psi_{jj} \rangle_{i \neq j} = \frac{\sigma^2}{15}, \quad \langle \Psi_{ij}^2 \rangle_{i \neq j} = \frac{2\sigma^2}{15}. \quad (55)$$

The joint PDF of the six components is therefore

$$\mathcal{P}(\Psi_{ij}) \propto \exp \left[ -\frac{15}{4\sigma^2} \left( \sum_i \Psi_{ii}^2 + \frac{1}{2} \sum_{i \neq j} \Psi_{ij}^2 - \frac{1}{5} \left( \sum_i \Psi_{ii} \right)^2 \right) \right]. \quad (56)$$

### Eigenvalue Decomposition and the Jacobian

Every real symmetric matrix can be diagonalized by an orthogonal transformation. Let  $\lambda_1 \geq \lambda_2 \geq \lambda_3$  be the ordered eigenvalues of  $\Psi_{ij}$ . Changing variables from the six independent components to the three eigenvalues plus three Euler angles  $\Omega$  that parametrise the diagonalising rotation, the Jacobian of the transformation is [25]

$$d^6 T = \prod_{i < j} |\lambda_i - \lambda_j| \cdot d\lambda_1 d\lambda_2 d\lambda_3 \cdot d\Omega, \quad (57)$$

where  $d\Omega$  is the Haar measure on  $SO(3)$ . Integrating over  $\Omega$  yields a constant that is absorbed into the normalization.

The exponent in (56), expressed in terms of eigenvalues, reads

$$\begin{aligned} & \sum_i \Psi_{ii}^2 + \frac{1}{2} \sum_{i \neq j} \Psi_{ij}^2 - \frac{1}{5} \left( \sum_i \Psi_{ii} \right)^2 \\ &= \sum_i \lambda_i^2 - \frac{1}{5} \left( \sum_i \lambda_i \right)^2. \end{aligned} \quad (58)$$

The joint PDF of the (unordered) eigenvalues is therefore

$$\mathcal{P}(\lambda_1, \lambda_2, \lambda_3) = \mathcal{N}_\lambda (\lambda_1 - \lambda_2)(\lambda_1 - \lambda_3)(\lambda_2 - \lambda_3) \times \exp \left[ -\frac{15}{4\sigma^2} \left( \sum_i \lambda_i^2 - \frac{1}{5} \left( \sum_i \lambda_i \right)^2 \right) \right], \quad (59)$$

where  $\mathcal{N}_\lambda = 15^3 / (8\pi\sqrt{5}\sigma^6)$  is the normalization in  $\lambda$ .

The characteristic polynomial of  $\Psi$  is  $\det(\lambda \mathbf{1} - \Psi) = \lambda^3 - I_1 \lambda^2 + I_2 \lambda - I_3$ , where the three *symmetric invariants* are

$$I_1 = \lambda_1 + \lambda_2 + \lambda_3 = \text{Tr } \Psi, \quad (60)$$

$$I_2 = \lambda_1 \lambda_2 + \lambda_1 \lambda_3 + \lambda_2 \lambda_3, \quad (61)$$

$$I_3 = \lambda_1 \lambda_2 \lambda_3 = \det \Psi. \quad (62)$$

A useful identity follows immediately,

$$\sum_i \lambda_i^2 = I_1^2 - 2I_2, \quad (63)$$

such that the exponent in (59) becomes

$$-\frac{15}{4\sigma^2} \left( \frac{4}{5} I_1^2 - 2I_2 \right) = -\frac{I_1^2}{2\sigma^2} - \frac{5(I_1^2 - 3I_2)}{2\sigma^2}. \quad (64)$$

The Jacobian  $|\Delta(\lambda)| = (\lambda_1 - \lambda_2)(\lambda_1 - \lambda_3)(\lambda_2 - \lambda_3)$  and the *discriminant*  $\Delta = \Delta(\lambda)^2$  are related to the  $I$ -invariants

$$\Delta = I_1^2 I_2^2 - 4I_2^3 - 4I_1^3 I_3 + 18I_1 I_2 I_3 - 27I_3^2. \quad (65)$$

Real, distinct eigenvalues require  $\Delta > 0$ .

### Marginalization over $I_3$

We change variables from  $(\lambda_1, \lambda_2, \lambda_3)$  to  $(I_1, I_2, I_3)$ . The Jacobian of this transformation is

$$\frac{\partial(\lambda_1, \lambda_2, \lambda_3)}{\partial(I_1, I_2, I_3)} = \frac{1}{|\Delta(\lambda)|}, \quad (66)$$

so the factor  $|\Delta(\lambda)|$  from the eigenvalue measure cancels the Jacobian, and the joint PDF in the  $I$ -invariants is

$$\mathcal{P}(I_1, I_2, I_3) = \frac{15^3}{8\pi\sqrt{5}\sigma^6} \exp \left( -\frac{I_1^2}{2\sigma^2} - \frac{5(I_1^2 - 3I_2)}{2\sigma^2} \right). \quad (67)$$

Treating  $I_1$  and  $I_2$  as fixed parameters,  $\Delta$  is a downward-opening quadratic in  $I_3$ :

$$\Delta(I_3) = -27I_3^2 + (18I_1 I_2 - 4I_1^3) I_3 + (I_1^2 I_2^2 - 4I_2^3). \quad (68)$$

The condition  $\Delta \geq 0$  (real eigenvalues) is satisfied between the two roots  $I_3^\pm$ , which are the physically allowed range of  $I_3$  for given  $(I_1, I_2)$ . Integrating the variable  $I_3$ ,

$$\int_{I_3^-}^{I_3^+} dI_3 = I_3^+ - I_3^- = \frac{4}{27} (I_1^2 - 3I_2)^{3/2}. \quad (69)$$

The marginal distribution in  $I_1$  and  $I_2$  is

$$\mathcal{P}(I_1, I_2) = \mathcal{N} (I_1^2 - 3I_2)^{3/2} \exp\left(-\frac{I_1^2}{2\sigma^2} - \frac{5(I_1^2 - 3I_2)}{2\sigma^2}\right), \quad (70)$$

with support in  $I_2 \leq I_1^2/3$  (real-eigenvalue condition), and normalization

$$\mathcal{N} = \frac{25\sqrt{5}}{2\pi\sigma^6}. \quad (71)$$

### Factorization via a Change of Variables

The key to computing the moments analytically is the substitution

$$u = I_1, \quad v = I_1^2 - 3I_2 \geq 0, \quad (72)$$

so that  $I_2 = (u^2 - v)/3$  and  $dI_1 dI_2 = \frac{1}{3} du dv$ .

The exponent transforms as

$$-\frac{I_1^2}{2\sigma^2} - \frac{5(I_1^2 - 3I_2)}{2\sigma^2} = -\frac{u^2}{2\sigma^2} - \frac{5v}{2\sigma^2}. \quad (73)$$

The distribution (70) in the new variables is given by

$$\mathcal{P}(u, v) = \frac{25\sqrt{5}}{6\pi\sigma^6} v^{3/2} \exp\left(-\frac{5v}{2\sigma^2} - \frac{u^2}{2\sigma^2}\right), \quad (74)$$

with  $u \in (-\infty, \infty)$ ,  $v \geq 0$ . The joint distribution (74) factorizes completely:  $u = I_1$  and  $v = I_1^2 - 3I_2$  are independent random variables. Their marginal distributions  $\mathcal{P}(u, v) = \mathcal{P}_u(u) \cdot \mathcal{P}_v(v)$  are properly normalized:

$$\mathcal{P}_u(u) = \frac{1}{\sigma\sqrt{2\pi}} \exp\left(-\frac{u^2}{2\sigma^2}\right), \quad \text{Gaussian} \quad (75)$$

$$\mathcal{P}_v(v) = \frac{25\sqrt{5}}{3\sigma^5\sqrt{2\pi}} v^{3/2} \exp\left(-\frac{5v}{2\sigma^2}\right), \quad \text{Gamma} \quad (76)$$

### Computation of the Moments $\langle I_1^2 \rangle$ and $\langle I_2 \rangle$

The fact that  $(u, v)$  are independent random variables allows us to compute the moments straightforwardly,

$$\langle u^{2n} \rangle = (2\sigma^2)^n \frac{\Gamma[1/2 + n]}{\Gamma[1/2]} \quad (77)$$

$$\langle v^n \rangle = \left(\frac{2\sigma^2}{5}\right)^n \frac{\Gamma[5/2 + n]}{\Gamma[5/2]}. \quad (78)$$

In particular,

$$\langle I_1^2 \rangle = \langle u^2 \rangle = \sigma^2, \quad (79)$$

$$\langle I_2 \rangle = \frac{1}{3}\langle u^2 \rangle - \frac{1}{3}\langle v \rangle = \frac{2\sigma^2}{15}. \quad (80)$$

The ratio  $\langle I_2 \rangle / \langle I_1^2 \rangle = 2/15$  is a universal prediction of Gaussian random field theory for the statistics of tidal deformation in the early Universe.

In particular,

$$\langle \log v \rangle = \frac{8}{3} - \gamma + \log \frac{\sigma^2}{10}, \quad (81)$$

where  $\gamma = 0.5772\dots$  is the Euler constant.

- 
- [1] J. R. Bond, L. Kofman, and D. Pogosyan, *Nature* **380**, 603 (1996), arXiv:astro-ph/9512141.
  - [2] V. Springel, C. S. Frenk, and S. D. M. White, *Nature* **440**, 1137 (2006), arXiv:astro-ph/0604561.
  - [3] Y. B. Zel'dovich, *Astronomy & Astrophysics* **5**, 84 (1970).
  - [4] O. Hahn, C. Porciani, C. M. Carollo, and A. Dekel, *Mon. Not. Roy. Astron. Soc.* **375**, 489 (2007), arXiv:astro-ph/0610280.
  - [5] M. Cautun, R. van de Weygaert, and B. J. T. Jones, *Mon. Not. Roy. Astron. Soc.* **429**, 1286 (2013), arXiv:1209.2043 [astro-ph.CO].
  - [6] A. Hosoya, T. Buchert, and M. Morita, *Phys. Rev. Lett.* **92**, 141302 (2004), arXiv:gr-qc/0402076.
  - [7] B. Pandey and S. Sarkar, *Mon. Not. Roy. Astron. Soc.* **454**, 2647 (2015), arXiv:1507.03124 [astro-ph.CO].
  - [8] B. Pandey, *Mon. Not. Roy. Astron. Soc.* **430**, 3376 (2013), arXiv:1301.4961 [astro-ph.CO].
  - [9] F. Leclercq, G. Lavaux, J. Jasche, and B. Wandelt, *Journal of Cosmology and Astroparticle Physics* **08**, 027 (2016), arXiv:1606.06758 [astro-ph.CO].
  - [10] B. L. Falck, M. C. Neyrinck, and A. S. Szalay, *Astrophys. J.* **754**, 126 (2012), arXiv:1201.2353 [astro-ph.CO].
  - [11] B. C. Coutinho, S. Hong, K. Albrecht, A. Dey, A.-L. Barabási, P. Torrey, M. Vogelsberger, and L. Hernquist, arXiv e-prints (2016), arXiv:1604.03236 [astro-ph.CO].
  - [12] F. Vazza, *Mon. Not. Roy. Astron. Soc.* **465**, 4942 (2017), arXiv:1611.09348 [astro-ph.CO].
  - [13] F. Vazza, *Mon. Not. Roy. Astron. Soc.* **491**, 5447 (2020), arXiv:1911.11029 [astro-ph.CO].
  - [14] J. Gaite, *Advances in Astronomy* **1**, 1 (2019).
  - [15] T. Bonnaire, N. Aghanim, J. Kuruvilla, and A. Decelle, *Astronomy & Astrophysics* **661**, A146 (2022), arXiv:2112.03926 [astro-ph.CO].
  - [16] C. E. Shannon, *Bell Syst. Tech. J.* **27**, 379 (1948).
  - [17] T. M. Cover and J. A. Thomas, *Elements of Information Theory*, 2nd ed. (Wiley-Interscience, Hoboken, NJ, 2006).
  - [18] B. B. Mandelbrot, *The Fractal Geometry of Nature* (W. H. Freeman, New York, 1982).
  - [19] V. J. Martínez and E. Saar, *Statistics of the Galaxy Distribution* (Chapman & Hall/CRC, Boca Raton, FL, 2002).
  - [20] A. G. Doroshkevich, *Astrophysics* **6**, 320 (1970).
  - [21] A. G. Doroshkevich and S. F. Shandarin, *Soviet Astronomy* **22**, 653 (1978).
  - [22] J. M. Bardeen, J. R. Bond, N. Kaiser, and A. S. Szalay, *Astrophysical Journal* **304**, 15 (1986).
  - [23] J. Lee and U.-L. Pen, *Astrophysical Journal Letters* **532**, L5 (2000), arXiv:astro-ph/9911328.
  - [24] D. Pogosyan, J. R. Bond, L. Kofman, and J. Primack, *Large Scale Structure: Tracks and Traces*, World Scientific, 61 (1998), arXiv:astro-ph/9810072.

- [25] M. L. Mehta, *Random Matrices*, 3rd ed. (Elsevier/Academic Press, Amsterdam, 2004).
- [26] P. J. E. Peebles, *The Large-Scale Structure of the Universe* (Princeton University Press, Princeton, NJ, 1980).
- [27] H. G. E. Hentschel and I. Procaccia, *Physica D* **8**, 435 (1983).
- [28] T. C. Halsey, M. H. Jensen, L. P. Kadanoff, I. Procaccia, and B. I. Shraiman, *Physical Review A* **33**, 1141 (1986), [Erratum: *Phys.Rev.A* 34, 1601 (1986)].
- [29] D. Alonso, A. Bueno belloso, F. J. Sánchez, J. García-Bellido, and E. Sánchez, *Mon. Not. Roy. Astron. Soc.* **440**, 10 (2014), arXiv:1312.0861 [astro-ph.CO].
- [30] M. Cautun, R. van de Weygaert, B. J. T. Jones, and C. S. Frenk, *Mon. Not. Roy. Astron. Soc.* **441**, 2923 (2014), arXiv:1401.7866 [astro-ph.CO].
- [31] V. Springel *et al.*, *Nature* **435**, 629 (2005), arXiv:astro-ph/0504097.
- [32] V. Springel *et al.*, *Mon. Not. Roy. Astron. Soc.* **475**, 676 (2018), arXiv:1707.03397 [astro-ph.GA].
- [33] P. Coles and B. Jones, *Mon. Not. Roy. Astron. Soc.* **248**, 1 (1991).
- [34] F. Bernardeau, *Astrophysical Journal* **433**, 1 (1994), arXiv:astro-ph/9312026.
- [35] F. Bernardeau, S. Colombi, E. Gaztañaga, and R. Scoccimarro, *Physics Reports* **367**, 1 (2002), arXiv:astro-ph/0112551.
- [36] A. A. Klypin, S. Gottlober, and A. V. Kravtsov, *Astrophys. J.* **516**, 530 (1999), arXiv:astro-ph/9708191.
- [37] E. V. Linder, *Phys. Rev. D* **72**, 043529 (2005), arXiv:astro-ph/0507263.
- [38] F. Leclercq, J. Jasche, and B. Wandelt, *JCAP* **06**, 015 (2015), arXiv:1502.02690 [astro-ph.CO].
- [39] J. Jasche and B. D. Wandelt, *Mon. Not. Roy. Astron. Soc.* **432**, 894 (2013), arXiv:1203.3639 [astro-ph.CO].
- [40] N. Porqueres, A. Heavens, D. Mortlock, and G. Lavaux, *Mon. Not. Roy. Astron. Soc.* **502**, 3035 (2021), arXiv:2011.07722 [astro-ph.CO].
- [41] DESI Collaboration, A. Aghamousa, *et al.*, arXiv e-prints (2016), arXiv:1611.00036 [astro-ph.IM].
- [42] R. Laureijs, J. Amiaux, S. Arduini, *et al.*, arXiv e-prints (2011), arXiv:1110.3193 [astro-ph.CO].
- [43] Ž. Ivezić, S. M. Kahn, J. A. Tyson, *et al.* (LSST), *Astrophysical Journal* **873**, 111 (2019), arXiv:0805.2366 [astro-ph].
- [44] F.-S. Kitaura, *Emergence of Complex Structures* (2026), arXiv:2604.11481 [astro-ph.CO].